Numerical and Experimental Investigations of Self-piercing Riveting

Xiaocong He[1)], Baoying Xing[1)], Kai Zeng[1)], Fengshou Gu [2)], Andrew Ball [2)]

1) Innovative Manufacturing Research Centre, Kunming University of Science and Technology, Kunming, 650093, P. R. China

2) Centre for Efficiency and Performance Engineering, University of Huddersfield, Queensgate, Huddersfield, HD1 3DH, UK.

Abstract

Self-pierce riveting (SPR) is a new high-speed mechanical fastening technique which is suitable for point joining dissimilar sheet materials, as well as coated and pre-painted sheet materials. With increasing application of SPR in different industrial fields, the demand for a better understanding of the knowledge of static and dynamic characteristics of the SPR joints is required. In this paper, the SPR process has been numerically simulated using the commercial finite element (FE) software LS-Dyna. For validating the numerical simulation of the SPR process, experimental tests on specimens made of aluminium alloy have been carried out. The online window monitoring technique was introduced in the tests for evaluating the quality of SPR joints. Good agreements between the simulations and the tests have been found, both with respect to the force-travel (time) curves as well as the deformed shape on the cross-section of SPR joint. Monotonic tensile tests were carried out to measure the ultimate tensile strengths for SPR joints with different material combinations. Deformation and failure of the SPR joints under monotonic tensile loading were studied. The normal hypothesis tests were performed to examine the rationality of the test data. This work was also aimed at evaluating experimentally and comparing the strength and energy absorption of SPR joints and SPR-bonded hybrid joints.

Keywords Self-piercing riveting; Process simulation; Finite element method; Testing; Process Monitoring.

1 Introduction

The use of Self-pierce riveting (SPR) is of great interest to many industrial sectors including aerospace and automotive, as well as packaging and domestic appliance (white goods) industries. This, together with increasing use of light weight materials which normally are difficult or impossible to weld, has produced a significant increase in the use of SPR technology in engineering structures and components in recent years [1, 2].

There have been a few published results on the static and dynamic properties of the SPR joints in the past few years. Wood et al. [3] investigated the performance of self-piercing riveted joints in aluminium sheet (A5754) at typical automotive crash speeds. Critical to the findings reported in this paper was the design of the fixture and force transducer to test U shaped tension specimens over the speed range of interest. A finite element (FE) model of the fixture and test measurement system was developed to ensure a near optimal design. Sufficient details of these were given to reproduce the test results. Durandet et al. [4] studied the laser-assisted SPR (LSPR) of AZ31 magnesium alloy strips. A simple but effective thermal analysis of LSPR was presented that enabled both the absorption of the laser radiation and heat transfer between plies to be determined. It was found that crack-free joints were produced at strip temperatures above 200°C at the time of rivet insertion. Using Forge2005® FE software, Bouchard et al. [5] modeled large deformation of elastic–plastic materials for 2D and 3D configurations. They found that it is possible to export the mechanical fields of a 2D simulation onto a 3D mesh using an interpolation technique, and then to perform a 3D shearing test on the riveted structure. Casalino et al. [6] proposed equations for governing the onset and propagation of crack, the plastic deformation, the space discretization, the time integration, and the contact evolution during the SPR process. A case study of the SPR of two sheets of the 6060T4 aluminum alloy with a steel rivet was performed using the LS-Dyna FE code. Hoang et al. [7] investigated the possibility of replacing steel self-piercing rivets with aluminum ones, when using a conventional die in accordance with the Boellhoff standards. An experimental program was carried out. The test results were exploited in terms of the riveting force–displacement curves and cross-sectional geometries of the riveted joints. The comparison analysis has been performed by Mucha [8] within the FE numerical experiment range to cover the effect of various riveting process parameters on the rivet deformation. Proper selection of corresponding rivet material features enables significant changing of the sheet joining process and specific finished joint parameters.

In this paper, the SPR process has been numerically simulated using the commercial FEA software LS-Dyna. A two dimensional axisymmetric model was generated based on the Cowper-Symonds material models. An implicit solution

technique with Lagrange method and r-self-adaptivity has been used. For validating the numerical simulation of the SPR process, experimental tests on specimens made of aluminium alloy 5754 have been carried out. The window technique was used in the tests for evaluating the quality of SPR joints. The structural analysis has been also performed for comparing the strength and energy absorption of SPR joints and SPR-bonded hybrid joints.

2 SPR Process Simulation

In SPR process, a semi-tubular rivet is pressed by a punch into two or more sheets of materials that are supported on a die. The die shape causes the rivet to flare inside the bottom sheet to form a mechanical interlock. In this study, the SPR process has been numerically simulated using the commercial FE software LS-Dyna. A two dimensional axisymmetric model was generated. Since SPR process involves large deformation, finite elements may become severely distorted. Distorted meshes are less accurate and may accordingly introduce numerical difficulties. In order to avoid numerical problems due to mesh disturbances, the efficacious approach is to use an erosion or element kill technique, where elements simply are removed from the mesh in accordance with a failure criterion. When the elements are removed, the interface between the sheets and the rivet becomes rough. In order to get a smoother interface, a small element size is required. However, a small element size increases the number of elements in the simulation and the time of the simulation. To take the whole situation into account, an implicit solution technique with Lagrange method and r-self-adaptivity has been used.

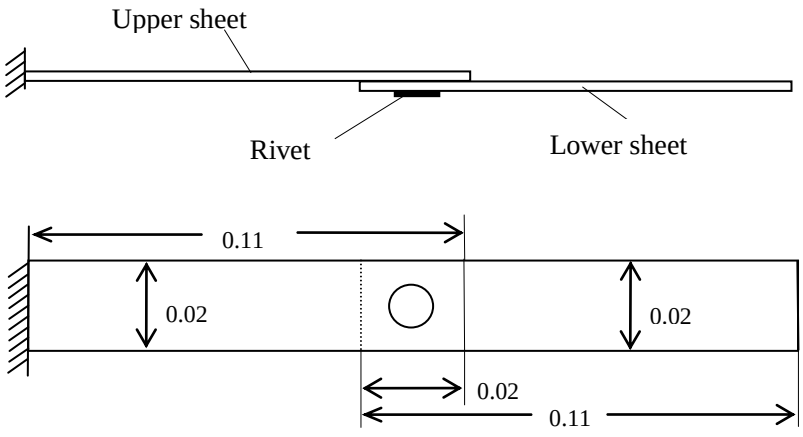

Fig. 1. A single lap SPR joint

The single lap SPR joint comprises an upper sheet, lower sheet and rivet as shown in Fig. 1. The sheet materials tested were 5754 aluminium alloy plates of dimensions

110 mm length ×20 mm width ×2 mm thickness and were joined together in the central part of lap section with one rivet. The rivet is made of high strength steel and is of dimensions 0.0055 m long ×0.005 m diameter. The mechanical properties of the materials show in Table 1.

Table 1 Material parameters

Material	Young's modulus (MPa)	Poisson's ratio	Yield stress (MPa)	Ultimate stress (MPa)	Elongation at failure [%]
Rivet	189000	0.30	1520.0	1720.0	22
Al5754	70300	0.33	114.0	250.0	24
Adhesive	1320	0.41		30	32.8

The punch, blank holder and die were modelled as rigid bodies, while the material of the rivet and the sheets were modelled as elasto-plastic materials, adopting the von Mises yield criterion, a piecewise linear isotropic strain-hardening rule, and the associated flow rule in the plastic domain. Fig. 2 shows the FE model of SPR process.

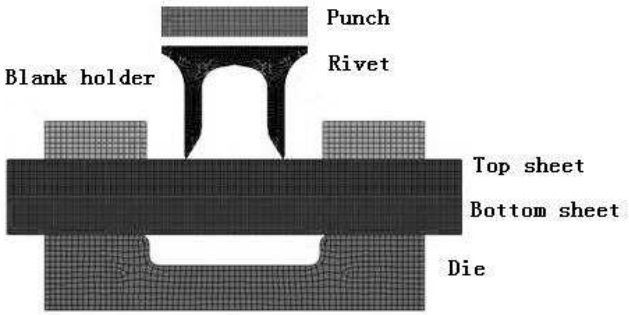

Fig. 2. FE model of SPR process

The friction between different parts in the model has an influence on the results of the simulation and the best value of the friction is not consistent for all the simulations. In the lack of experimental data, tentative values of the Coulomb friction coefficient between different parts in the model were assumed as follows: f=0.25 punch-rivet, f=0.25 rivet-upper sheet, f=0.25 rivet-lower sheet, f=0.15 upper sheet-blank holder, f=0.15 upper sheet-lower sheet, f=0.25 lower sheet-die. These values were kept constant for all simulations in this study.

To save CPU time, start the analysis at the moment when the rivet touch the top surface of the upper substrate and apply a specified initial velocity to simulate the SPR process. The SPR process is modelled by applying a downward initial velocity to every node within the punch. Fig. 3 shows SPR process FE simulation and Fig. 4 shows the pressure-time curve of typical element in the simulation.

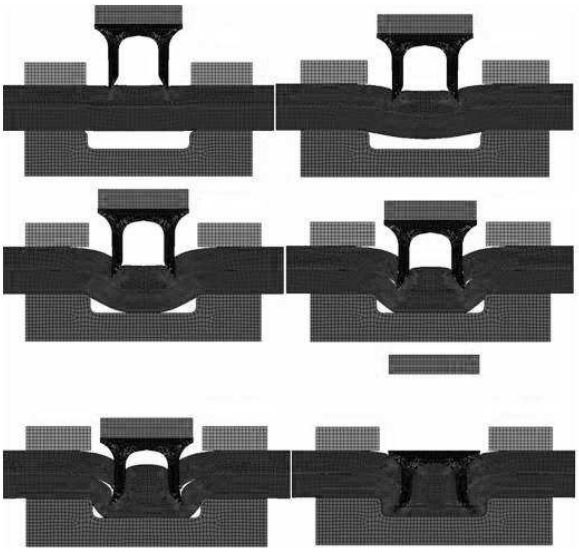

Fig. 3. FE simulation of SPR process

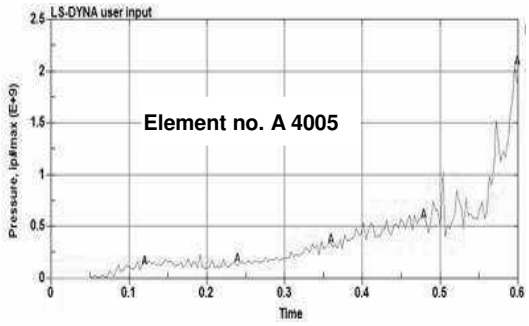

Fig. 4. Pressure-time curve in SPR process simulation

3 SPR process tests and online window monitoring

A RIVSET MTF Self Pierce Rivet system was employed as SPR machine as shown in fig. 5. A window monitoring system is mounted in the machine. The online window monitoring of SPR process is carried out by measuring actual SPR setting force through a force sensor and punch travel through a position sensor. The SPR setting force reflects the deformation force on the sheet materials and the punch travel indicated the geometric change of the sheets during SPR process. Signals obtained from sensors are amplified and transferred to the data acquisition system which measures, processes and saves the signals. A computer is used to save the measured data and generate the force-travel curves. All SPR joints were made with constant pre-clamp (5 kN) and setting (40 kN) load.

Fig. 5. Test set up of process window monitoring of SPR process

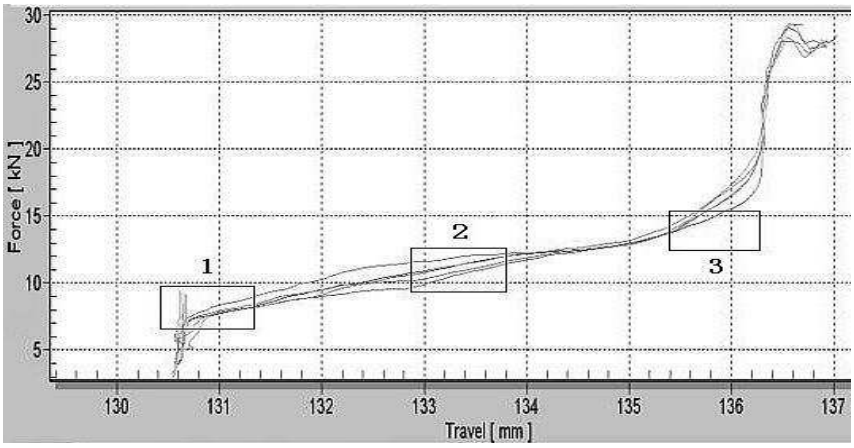

Fig. 6. Monitoring force-travel curves of SPR process

A reference force-travel curve must be established under the standard work conditions before the monitoring process. The SPR joint could be supposed to be of good quality under these conditions. As shown in Fig. 6, three windows are established depending on the features of the force-travel curve. The window 1 is set at the area where the rivet is piercing the top sheet; the window 2 at the area where the rivet is penetrating into the bottom sheet and the window 3 at the area where the rivet is flaring in the bottom sheet. The in and out directions for the force-travel curve through the windows are designed as follows: for the window 1 the curve should go in from bottom and out from right side; for the window 2 the curve should thread it from left side to right side and for the window 3 the curve should go in from left side and out from top side. In the SPR process online monitoring, if a measured force-travel curve goes through these set windows in the above procedure, the quality of the

corresponding SPR joint will be evaluated as right. On the other hand, if a measured curve goes through the windows in any other ways, the quality of the corresponding joint may not be as good as defined. It is obviously that under the same work conditions, the monitoring force-travel curves should nearly the same, as shown in Fig. 6.

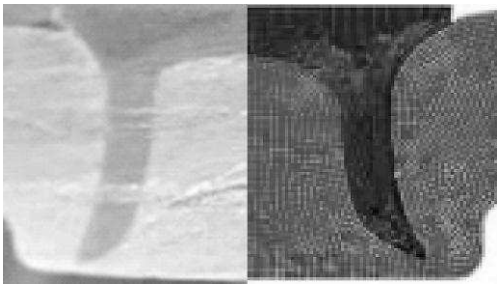

Fig. 7. Cross-section comparison

Fig. 7 shows the cross-section comparison between simulations and tests of SPR processes. Good agreements between the simulations and the tests have been found, both with respect to the force-travel (time) curves as well as the deformed shape on the cross-section. The results show the capability to simulate the SPR process for different geometries and work conditions.

4 Deformation and failure of SPR joints

SPR has found applications in heavy-duty situation, such as car bodies. Load-bearing capacity and energy absorption are two most important features in SPR joints structural analysis. It is also important for SPR to benefit from the advantages of other joining techniques, such as adhesively bonding. It is commonly understood that the addition of adhesive in SPR joints is beneficial but it is not clear if there are negative effects on mechanical properties of SPR joints [9]. Deformation and failure of homogeneous joints under monotonic tensile loading were studied for validating the load-bearing capacity and energy absorption of the bonded joins, SPR joints and SPR-bonded hybrid joints.

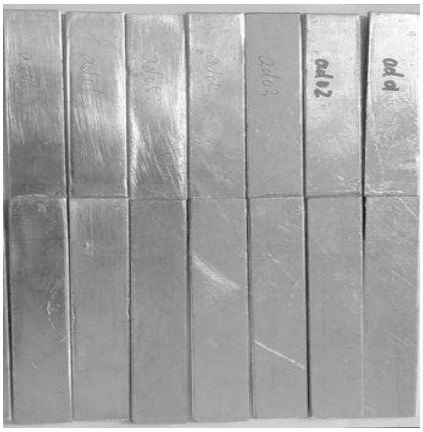

(a) Bonded joints

(b) SPR joints

(c) SPR-bonded hybrid joints

Fig. 8. Bonded joints, SPR joints and SPR-bonded hybrid joints

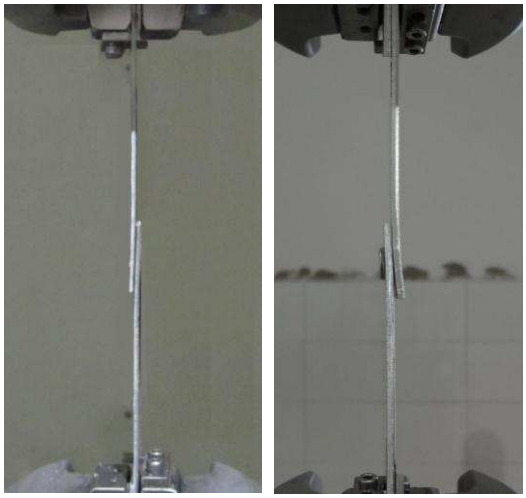

(a) Bonded joint (b) SPR joint

Fig. 9. Monotonic tensile process

The SPR-bonded hybrid joints were produced following exactly the same procedure as the respective SPR joints. The adhesive was applied on degreased surfaces and the two sheets were pressed together in order to squeeze sufficient adhesive out to avoid undue quilting of the finished SPR-bonded hybrid joints. The SPR joints were then produced. The thickness of the adhesive layer was controlled by the SPR process and was estimated to be 0.1 mm. Thereafter, the adhesive was cured at room temperature for at least 24 hours. Fig. 8 shows the bonded joins, SPR joints and SPR-bonded hybrid joints.

A servo-hydraulic testing machine with hydraulic grips was used for conducting the tests. The grip to grip specimen length was about 100 mm. The upper end of the joints was fixed, and a quasi-static downward displacement was applied to the lower end. The tests were performed with a constant displacement rate of 1 mm/min. Continuous records of the applied force-displacement curves were obtained during each test. Figures 9 and 10 show the monotonic tensile process and failed joints. It can be seen from figures 9 and 10 that the failure mode was plate failure forming at the contact location between the rivet bottom and the lower sheet. In the test, plastic deformation around contact location developed to such a large level that the rivet was pulled out from the lower sheet.

Fig. 11 shows the force-displacement curves of the bonded joins, SPR joints and SPR-bonded hybrid joints. For each test, seven samples were mechanically tested. To examine the rationality of the test data, the normal hypothesis tests were performed using MATLAB 7.0. The results show that the tensile strengths of all the bonded joins,

SPR joints and SPR-bonded hybrid joints follow normal distributions. The mean values (μ) and standard deviations (σ) have the following numerical values: for bonded joints μ_{Ad} =397.20 N, σ_{Ad} =89.00 N; for SPR joints μ_{SPR} =2646.40 N, σ_{SPR} =209.10 N; for SPR-bonded joints $\mu_{SPR\text{-}Ad}$ =3071.00 N, $\sigma_{SPR\text{-}Ad}$ =177.10 N. All test data fitting the region estimated by the degree of confidence of 95%. The tensile strengths normal probability density distributions of the bonded joints, SPR joints and SPR-bonded hybrid joints are also showed in Fig. 11.

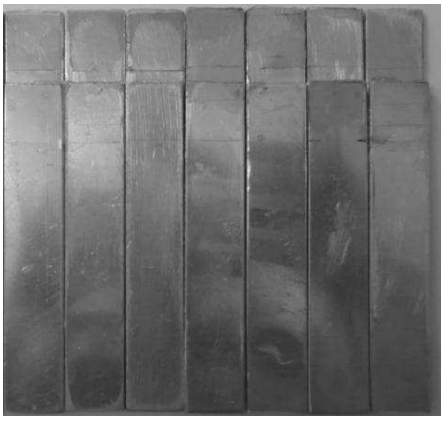

(a) Failed bonded joints

(b) Failed SPR joints

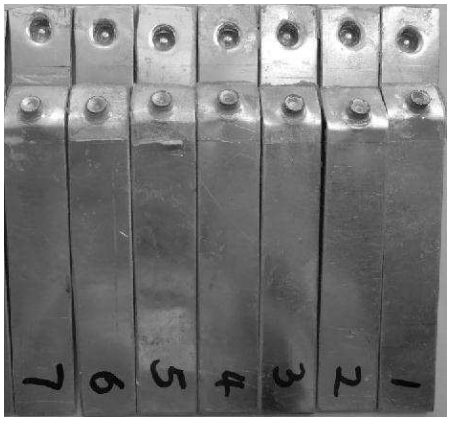

(c) Failed SPR-bonded hybrid joints

Fig. 10. Failed bonded joints, SPR joints and SPR-bonded hybrid joints

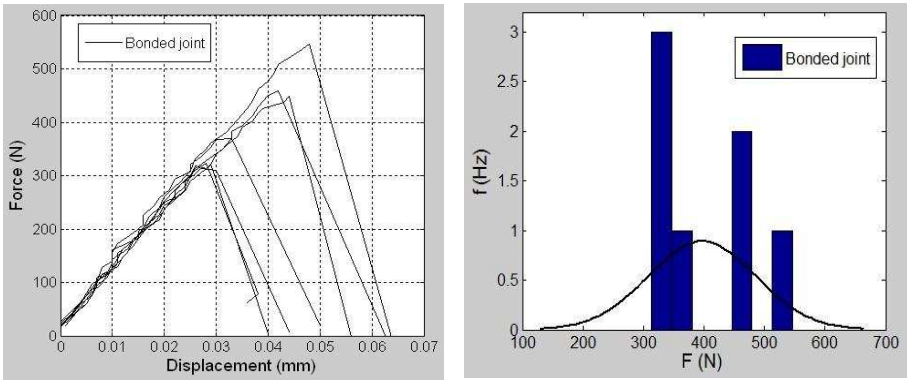

(a) Bonded joints

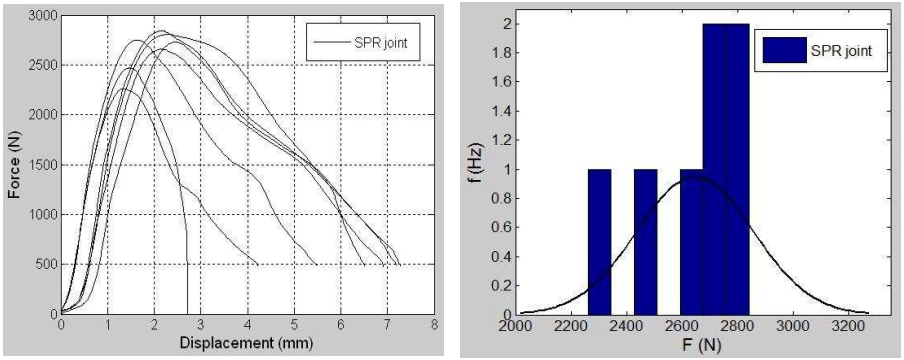

(b) SPR joints

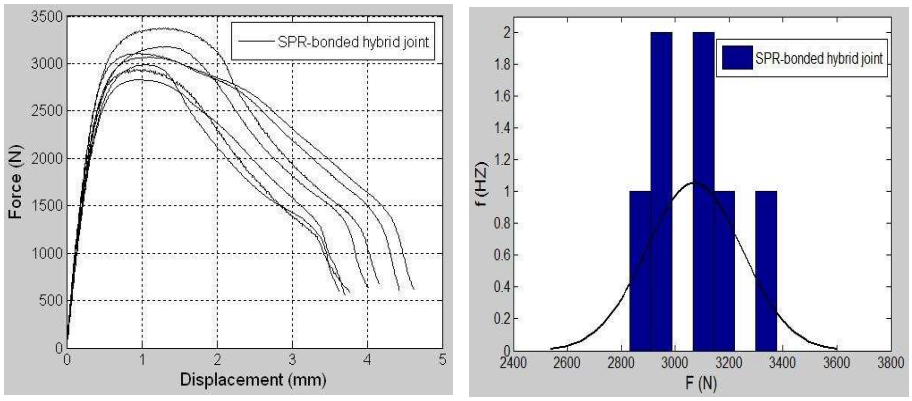

(c) SPR-bonded hybrid joints

Fig. 11. Force-displacement curves and tensile strengths normal probability density distributions of bonded joints, SPR joints and SPR-bonded hybrid joints

It can be seen from Fig. 11 that the results proved to be reproducible and therefore only one typical curve is shown in the Fig. 12 for each of the test. In this figure, solid line represents the force-displacement of bonded joint. Dotted line denotes SPR joint and dash-dot line denotes SPR-bonded hybrid joint. In the case of bonded joint, after the peak the force suddenly drops to zero. In the cases of SPR-bonded joint, after the

peak the force decreases rapidly. In the case of SPR joint, however, after the peak the force decreases gradually. Obviously the failure processes of SPR and SPR-bonded joints involve much higher energy absorptions with respect to bonded joint.

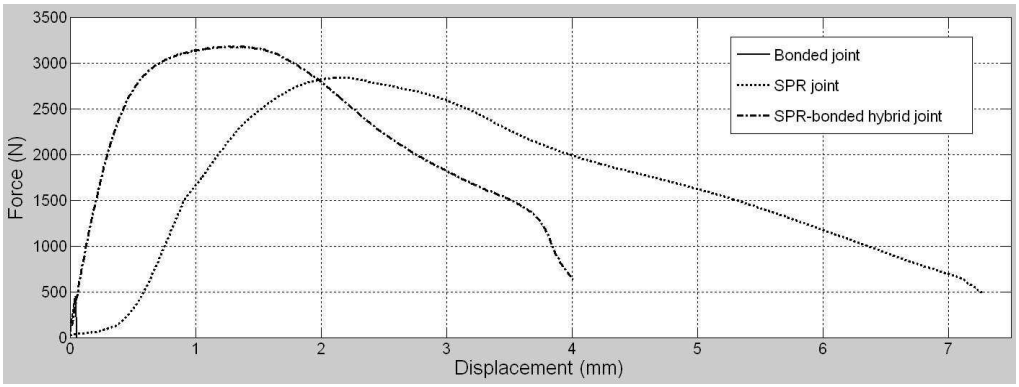

Fig. 12. Typical force-displacement curves of bonded joints, SPR joints and SPR-bonded hybrid joints

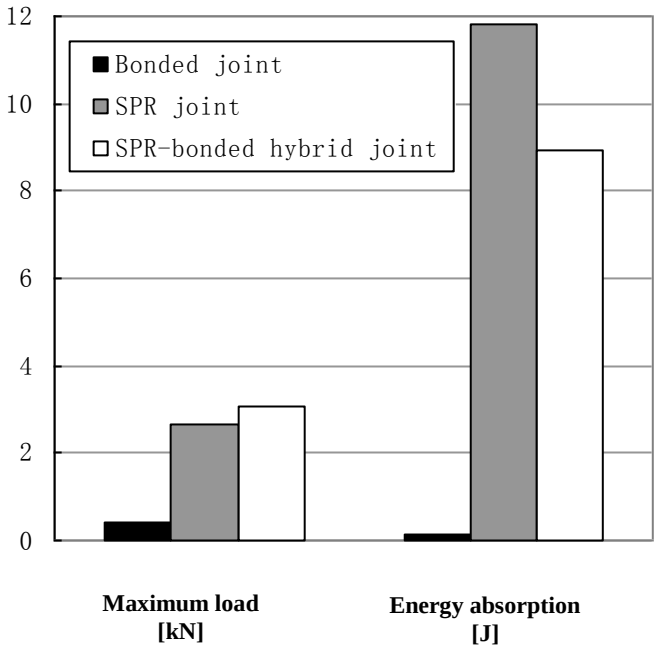

Fig. 13. Intercepts of strength and energy absorption for bonded joints, SPR joints and SPR-bonded hybrid joints

Fig. 13 shows the intercept for load-bearing capacity and energy absorption of the bonded joints, SPR joints and SPR-bonded hybrid joints. It is worth noticing that the maximum load of SPR-bonded joint is 14% higher than that of SPR joint, but the energy absorption is 24% lower than that of SPR joint. This means that the addition of

adhesive in SPR joint resulted in an increase in the yield and failure loads but a decrease in the energy absorption of SPR joints. This phenomenon can be attributed to adhesive layers located in the interfaces between the rivet and different parts. The failure of adhesive layer occurred in a brittle manner, the presence of adhesive layer could not contribute to any significant increase in the total potential for energy absorption of the SPR-bonded hybrid joint. On the contrary, the adhesive layers decrease the friction coefficient between the rivet and different parts and make it easier for the rivet pulling out from joint when the failure occurs.

5 Summary

Self-piercing riveting (SPR) is a high-speed mechanical fastening technique which is suitable for point joining advanced lightweight sheet materials that are dissimilar, coated and hard to weld. The SPR process has been numerically simulated in this paper using the commercial finite element (FE) software LS-Dyna. Experimental tests on specimens made of aluminium alloy 5754 have been carried out for validating the numerical simulation of the SPR process. The window technique was used in the tests for evaluating the quality of SPR joints. Signals obtained from sensors were amplified and transferred to the data acquisition system which measures, processes and saves the signals. Good agreements between the simulations and the tests have been found, both with respect to the force-travel (time) curves as well as the deformed shape on the cross-section of SPR joint. Deformation and failure of homogeneous joints under monotonic tensile loading were studied for validating the load-bearing capacity and energy absorption of the bonded joints, SPR joints and SPR-bonded hybrid joints.

Acknowledgement

This study is partially supported by National Science Foundation of China (Grant No. 50965009)

References

[1] He X, Gu F, Ball A (2012) Recent Development in Finite Element Analysis of Self-piercing Riveted Joints. Int J Adv Manuf Technol 58: 643-649

[2] He X, Pearson I, Young K (2008) Self-pierce riveting for sheet materials: State of the art. J Mater Process Technol 199: 27-36

[3] Wood PKC, Schley CA, Williams MA, Rusinek A (2011) A model to describe the high rate performance of self-piercing riveted joints in sheet aluminium. Mater Des 32: 2246-2259

[4] Durandet Y, Deam R, Beer A, Song W, Blacket S (2010) Laser assisted self-

pierce riveting of AZ31 magnesium alloy strips. Mater Des 31: S13–S16
[5] Bouchard PO, Laurent T, Tollier L (2008) Numerical modeling of self-pierce riveting—from riveting process modeling down to structural analysis. J Mater Process Technol 202: 290-300
[6] Casalino G., Rotondo A, Ludovico A (2008) On the numerical modeling of the multiphysics self piercing riveting process based on the finite element technique. Adv Engg Software 39(9): 787-795
[7] Hoang NH, Porcaro R, Langseth M, Hanssen AG (2010) Self-piercing riveting connections using aluminum rivets. Int J Solids Struct 47(3-4): 427–439
[8] Mucha J (2011) A study of quality parameters and behaviour of self-piercing riveted aluminium sheets with different joining conditions. Strojniski Vestnik/J Mech Engg 57: 323-333
[9] He X (2011) A review of finite element analysis of adhesively bonded joints. Int J Adhes Adhes 31: 248-264